SCIENCE CHINA
Earth Sciences

•RESEARCH PAPER•

April 2022 Vol.65 No.4: 759–768
https://doi.org/10.1007/s11430-021-9917-0

The solar wind plasma upstream of Mars observed by Tianwen-1: Comparison with Mars Express and MAVEN

Kai FAN[1,2], Limei YAN[1,2], Yong WEI[1,2*], Aibing ZHANG[3,4,5], Linggao KONG[3,4,5], Markus FRÄNZ[6], Fei HE[1,2], Lihui CHAI[1,2], Chongjing YUAN[1,2], Yuqi WANG[1,2], Jun ZHONG[1,2], Zhaojin RONG[1,2], Zhonghua YAO[1,2], Yongxin PAN[1,2], Jun CUI[8], Jiansen HE[9], Wenya LI[3,7], Binbin TANG[3,7] & Chi WANG[3,7]

[1] *Key Laboratory of Earth and Planetary Physics, Institute of Geology and Geophysics, Chinese Academy of Sciences, Beijing 100029, China;*
[2] *College of Earth and Planetary Sciences, University of Chinese Academy of Sciences, Beijing 100049, China;*
[3] *National Space Science Center, Chinese Academy of Sciences, Beijing 100190, China;*
[4] *Beijing Key Laboratory of Space Environment Exploration, Beijing 100190, China;*
[5] *Key Laboratory of Science and Technology on Space Environment Situational Awareness, Chinese Academy of Sciences, Beijing 100190, China;*
[6] *Max-Planck-Institute for Solar System Research, Goettingen 37077, Germany;*
[7] *State Key Laboratory of Space Weather, Chinese Academy of Sciences, Beijing 100190, China;*
[8] *School of Atmospheric Sciences, Sun Yat-Sen University, Zhuhai 519082, China;*
[9] *Institute of Space Physics and Applied Technology, Peking University, Beijing 100871, China*

Received December 15, 2021; revised February 15, 2022; accepted March 3, 2022; published online March 14, 2022

Abstract On the great journey to Mars, China's first planetary exploration mission, the Tianwen-1 came within 26 million kilometers of Mars from 31 October 2020 to 25 January 2021 and was getting closer to its destination, the red planet, in search of answers to the cataclysmic climate change that occurred in Martian history. Both the escape of the Martian atmosphere and the loss of surface water were firmly influenced by solar activities. Tianwen-1 provided a unique chance to depict the solar wind streams between Earth and Mars during the minimum of Solar Cycle 25. During the three-month cruise phase of Tianwen-1, the solar wind flows were successively observed at Earth, Tianwen-1, and Mars. After the field of view correction and noise reduction, the solar wind velocity and density measured by Tianwen-1 show good agreement with those at Earth and Mars. The results indicate that the performance of the ion analyzer onboard the Tianwen-1 orbiter is reliable and stable. It is worth looking forward to the joint observations of ion escape with other Mars probes in the following Martian years.

Keywords Tianwen-1, Mars, Plasma moment, Solar wind

Citation: Fan K, Yan L, Wei Y, Zhang A, Kong L, Fränz M, He F, Chai L, Yuan C, Wang Y, Zhong J, Rong Z, Yao Z, Pan Y, Cui J, He J, Li W, Tang B, Wang C. 2022. The solar wind plasma upstream of Mars observed by Tianwen-1: Comparison with Mars Express and MAVEN. Science China Earth Sciences, 65(4): 759–768, https://doi.org/10.1007/s11430-021-9917-0

1. Introduction

China's first successful planetary exploration program, the Tianwen-1, arrived at Mars on 10 February 2021. Tianwen-1 consists of an orbiter, a lander, and a rover named Zhurong. Tianwen-1 aspires to disclose the missing links between Martian ion escape processes and their consequences for Martian climate change (e.g., Wan et al., 2020a; Zou et al., 2021). Previously, the results based on former Martian missions limited the ion escape rate to account for only a few

*Corresponding author (email: weiy@mail.iggcas.ac.cn)

centimeters thickness of global water (e.g., Barabash et al., 2007). However, a burst of losses during intense solar activity from later observations puts the issue of ion losses back into a dispute (e.g., Jakosky et al., 2015a). Thus, the upstream solar winds which determine the space environment of Mars are crucial for understanding the evolution of the Martian atmosphere and water loss history (e.g., Lammer et al., 2008; Nilsson et al., 2021).

Besides the quiet flow with different velocities, there are also large-scale disturbances in the solar wind, such as the interplanetary coronal mass ejections (ICMEs) and stream interaction regions (SIRs). As propagating away from the Sun, the boundaries of the SIRs probably evolve into interplanetary shocks, which can accelerate charged particles to 20 MeV(e.g., Richardson, 2018). The SIRs can also modulate the galactic cosmic rays arriving at planets (e.g., Forbush, 1993; Simpson, 1998, and references therein) and the Jovian energetic electrons in the heliosphere (e.g., Conlon and Simpson 1977; Conlon, 1978; Ferreira et al., 2001). At Earth, the SIRs are also geoeffective and responsible for moderate and minor geomagnetic storms (e.g., Zhang et al., 2006; Chi et al., 2018).

Solar wind between Earth and Mars has been measured by the fly-bys of several previous spacecrafts, such as Voyager 1, Voyager 2 (e.g., Gazis, 1994), and Pioneer 11 (e.g., González-Esparza and Smith 1996) in the 1970s, Ulysses (e.g., Söding et al., 2001; Bavassano et al., 2001) from the 1990s to the 2000s, the Mars Atmosphere and Volatile EvolutioN (MAVEN) mission in the 2010s (e.g., Jakosky et al., 2015b). Unlike the Mars 2020 mission and the Hope Mars orbiter (e.g., Wan et al., 2020b), which were also launched in July 2020, Tianwen-1 is the only one of the three Mars Exploration missions that measured the solar wind plasma within 26 million kilometers upstream of Mars during its cruise phase. Observations in the solar wind through Tianwen-1 provide a valuable chance to monitor SIRs and ICMEs at the beginning of the solar cycle 25, it provides a unique chance to jointly measure the solar wind from Earth to Mars through OMNI, Tianwen-1, and MAVEN one after another during the same time window.

Zhang et al. (2022) presented the first results of the solar wind observation from MINPA and evaluated the blocking effect due to the lander capsule. Their study mainly used the energy flux of solar wind obtained by MINPA and showed the solar wind plasma moments only for a SIR event from 21 November 2020 to 22 November 2020. Here we focus on the calculation of the solar wind plasma moments with MINPA datasets in section 2 and the comparison of the derived solar wind velocity and density from MINPA observations with those from other solar wind data sets, such as OMNI, Mars Express, and MAVEN, which will be introduced in sections 3 and 4.

2. Data and methods

The Mars Ion and Neutral Particle Analyzer (MINPA) instrument onboard the Tianwen-1 orbiter is designed to detect ions and energetic neutral atoms (ENA) in the Martian space. MINPA is able to distinguish different ion species, such as H^+, He^+, O^+, O_2^+, and CO_2^+, and resolve proton and oxygen atoms from ENA measurements. MINPA provides ion data in the energy range of 2.8 eV to 25.9 keV, with a time resolution of 4 seconds (Kong et al., 2020). From July 2020 to October 2021, the scheduled MINPA working plan carried out a continuous measurement from 31 October 2020 to 25 January 2021 and three testing measurements on 23 March, 24 March, and 9 April 2021. Considering that Tianwen-1 arrived at Mars on 10 February 2021, MINPA has observed the solar wind during its first 3-months of measurements with a detection mode of 64 energy steps one mass step (only protons). The instrumental field of view is 360°×90°, dividing the hemispheric viewing field into 16 azimuthal angles (note as φ, each sector is 22.5° wide) multiplying 16 deflection angles (note as θ, each sector is 5.63° wide).

Figure 1 presents the orbits of Earth, Tianwen-1, and Mars, in the Heliocentric Aries ecliptic (HAE) coordinate system, in which the x-axis points from the center of the Sun to the first point of Aries, the z-axis is perpendicular to the ecliptic plane and pointing northward, and the y-axis completes a right-hand system (e.g., Fränz and Harper, 2002).

Besides the solar wind observation from Tianwen-1, we also used the solar wind observations near Earth and Mars. The hourly solar wind velocity and density near-Earth (King and Papitashvili, 2005) were obtained from the GSFC/SPDF

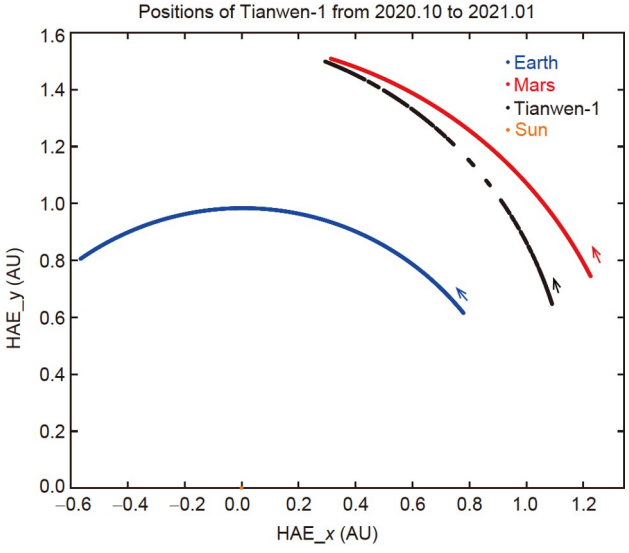

Figure 1 Positions of Tianwen-1 during the cruise phase from 31 October 2020 to 25 January 2021. The blue, black, red, and orange dots denote positions of Earth, Tianwen-1, Mars, and the Sun in the HAE coordinate system respectively. Small arrows mark the motion directions. The unit in each axis is the astronomical unit (AU), equal to the average distance between Earth and the Sun.

OMNIWeb. The solar wind velocity and density near Mars were from the Solar Wind Ion Analyzer (SWIA) and the Supra Thermal And Thermal Ion Composition (STATIC) instrument onboard MAVEN. SWIA and STATIC are 'top hat' electrostatic analyzers with a time resolution of 4 seconds. SWIA has no discrimination of ion species but has a good spatial resolution of protons from 25 eV to 25 keV (Halekas et al., 2015). STATIC provides ion data in the energy range of 0.1 eV to 30 keV, distinguishing ion species such as H^+, O^+, O_2^+ (McFadden et al., 2015). SWIA also provides ion moments data such as density and velocity in the MAVEN Level-2 database. In the discussion section, this work also used 12 years' observations of the solar wind near Mars measured through the Ion Mass Analyzer (IMA) from the Analyzer of Space Plasmas, and Energetic Atoms 3 (ASPERA-3) set onboard Mars Express (Barabash et al., 2006). IMA distinguishes different ion species from 10 eV to 30 keV, and provides ions moments data sampled over 192 seconds.

2.1 Noise reduction

The MINPA instrument is one of the seven scientific payloads onboard the Tianwen-1 orbiter. Zhang et al. (2022) conclude that nearly half of the signals are shadowed, which is responsible for the low-density values of the observations. The electronic noises need to be reduced to provide a more accurate plasma moment dataset. Figure 2 provides an example of the solar wind data measured on 1 November 2021. The looking direction of MINPA and the platform's status were also described in Zhang et al. (2022). During Tianwen-1's cruise phase, the contamination of instrumental noises is centered around 180° in azimuthal angles, and the noises could be removed through:

$$Data_{signal} = Data_{raw} - \frac{\sum_i Data_{noise}}{i}, \quad (1)$$

where i is the number of bins, we used 90 bins here to cover azimuthal angles from 135° to 225° in the looking directions.

After the reduction, observations of the solar wind's beam are centered near the top of the MINPA field of view region. However, as mentioned above, nearly half of the signals are still shadowed. This effect is responsible for the low-density values calculated from the cruise datasets, which need further analysis and are discussed in section 2.2.

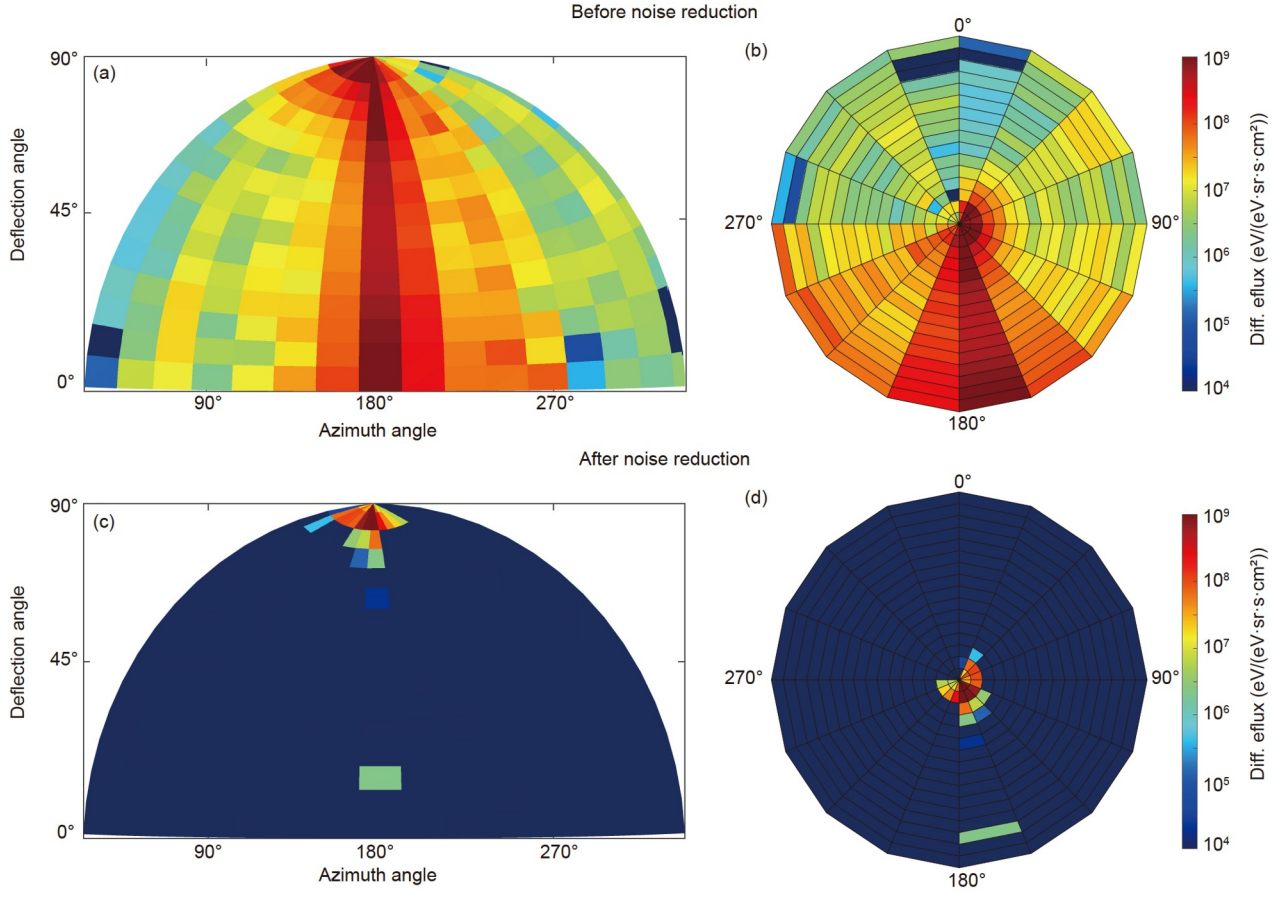

Figure 2 Observations of the solar wind on 1 November 2020. (a) & (b) provide the raw data measured through MINPA, and (c) & (d) show signals after the noise reduction. Grids represent the 16×16 solid angles, and the colors denote the measured differential energy fluxes in units of eV/(eV·sr·s·cm^2).

2.2 Calculation of the plasma moments

A general introduction to plasma moment calculation can be found in several textbooks (e.g., Hutchinson, 2002; Wuest et al., 2007). Methods used in this work follow a paper published by Fränz et al. (2006), which has been widely approved by application to observations by Mars Express (e.g., Dubinin et al., 2007; Wei et al., 2012) and MAVEN (e.g., Dubinin et al., 2020; Fan et al., 2020).

The plasma moments of a given particle species could be integrated through the distribution function, $f(v)$, in velocity space as:

$$\boldsymbol{M}^{i} = mf(\boldsymbol{v})\boldsymbol{v}^{i}d^{3}v, \tag{2}$$

where $\boldsymbol{M}$ is a tensor of order i, m is the mass of the given particles, d^3v is the volume element in velocity space. Then the number density (zero-order), the mass flux density vector (first-order), the momentum flux density tensor (second-order) is:

$$\boldsymbol{M}^{0} = n = mf(\boldsymbol{v})d^{3}v, \tag{3}$$

$$\boldsymbol{M}^{1} = n\boldsymbol{V} = mf(\boldsymbol{v})(\boldsymbol{v})d^{3}v, \tag{4}$$

$$\boldsymbol{M}^{2} = \boldsymbol{P} + n\boldsymbol{V}\boldsymbol{V} = mf(\boldsymbol{v})(\boldsymbol{v})(\boldsymbol{v})d^{3}v, \tag{5}$$

where n is the number density, $\boldsymbol{V}$ is the bulk velocity, $\boldsymbol{P}$ is the pressure tensor. And the plasma temperature could be calculated through $nkT = \mathrm{Tr}(\boldsymbol{P})/3$, where k is the Boltzmann constant. The relation between the distribution function and the differential flux $j(E,\Omega)$ for particles of energy (E) within a differential solid angle Ω is:

$$j(E,\Omega) = \frac{\boldsymbol{v}^2}{m}f(\boldsymbol{r},\boldsymbol{v}) = \frac{2E}{m^2}f(\boldsymbol{r},\boldsymbol{v}). \tag{6}$$

Using eq. (6), eqs. (3) and (4) could be rewritten as

$$n = \int \sin\varphi \mathrm{d}\varphi \int \mathrm{d}\theta \int \sqrt{\frac{m}{2E}} j(E,\varphi,\theta)\mathrm{d}E, \tag{7}$$

$$nV_x = \int \cos\varphi \mathrm{d}\varphi \int \sin^2\theta \mathrm{d}\theta \int j(E,\varphi,\theta)\mathrm{d}E, \tag{8}$$

$$nV_y = \int \sin\varphi \mathrm{d}\varphi \int \sin^2\theta \mathrm{d}\theta \int j(E,\varphi,\theta)\mathrm{d}E, \tag{9}$$

$$nV_z = \int \mathrm{d}\varphi \int \sin\theta\cos\theta \mathrm{d}\theta \int j(E,\varphi,\theta)\mathrm{d}E, \tag{10}$$

where φ and θ are azimuthal angles and deflection angles, respectively.

The plasma moments could also be calculated by assuming that the particle's phase space densities (PSD) fulfill the Maxwell-Boltzmann distribution in velocity space:

$$f(\boldsymbol{r},\boldsymbol{v}) = n\left(\frac{m}{2\pi k}\right)^{\frac{3}{2}} \mathrm{e}^{\left[-\frac{m(v-V)^2}{2kT}\right]}. \tag{11}$$

Using eq. (6), eq. (11) could be rewritten as

$$f(\boldsymbol{r},\boldsymbol{v}) = \frac{j(E,\Omega)m^2}{2E} = n\left(\frac{m}{2\pi E_t}\right)^{\frac{3}{2}} \mathrm{e}^{\left[-\frac{\left(\sqrt{E}-\sqrt{E_m}\right)^2}{E_t}\right]}. \tag{12}$$

Fitting the measured spectrum allows determining the particles' number density, thermal energy E_t, and mean energy E_m, respectively. A more detailed analysis could be found in Fränz et al. (2006), which presented "the first electron and ion moment maps (density, velocity, and temperature) of the Martian plasma environment, using data from the ELS and IMA sensors of the ASPERA-3 experiment on board Mars Express" (Fränz et al., 2006).

Nevertheless, the accuracy of the calculated moments through each method is restricted by MINPA's sheltered field of view. Figure 3 provides an example of the solar wind observations on 12 December 2020. From 6:00 to 19:00 UT, the solar wind plasma signals near 1 keV energy show clear enhancements, expecting an instrumental cessation happened between 14:29 UT to 15:43 UT. However, most of the obstructed energy fluxes and the blurry signals could still be seen near 2:00 or 21:00 UT. The PSDs measured through MINPA at 07:16 UT, 10:58 UT, and 17:53 UT are shown in Figure 4. Data are sampled over 4 seconds. Black lines are measured data while the others are fitted assuming a Gaussian distribution around the maximum of the spectrum. Generally, the sheltered field of view limits the width and intensity of fluxes. As a result, both the fitted peak and width might be underestimated, and it is necessary to compare the solar wind measurements of Tianwen-1 with other datasets such as the OMNI near Earth or MAVEN near Mars. The moment data are corrected for the influence of the spacecraft speed but without taking into account of the effect of the spacecraft potential.

3. Results

During the cruise phase of Tianwen-1 from 31 October 2020 to 25 January 2021, MINPA finished its first 3-months of measurements which accumulated unique solar wind plasma data from 25,765,773 km to 3,559,077 km upstream of Mars. Although the shadowing effect significantly amplified the attenuation of the instrument's field of view, MINPA could still complete its survey of the solar wind and capture the main property and variability of the solar wind. As for the limitation of the instrumental solid angles, much fewer particles would come into the detection field in the quiet solar wind. However, in the disturbed solar wind such as the SIRs, a larger positive transverse angle led to more particles detected by MINPA (Zhang et al., 2022). As illustrated in Figure 5, the differential energy fluxes of the solar wind show several strong enhancements, indicating that MINPA encounters several large-scale solar wind disturbances.

After the preparation of picking fine PSD cases with a sharp energy peak automatically, densities within the red dash frames in Figure 5 are clustered and plotted in Figure 6b. The solar wind velocity and density are compared at

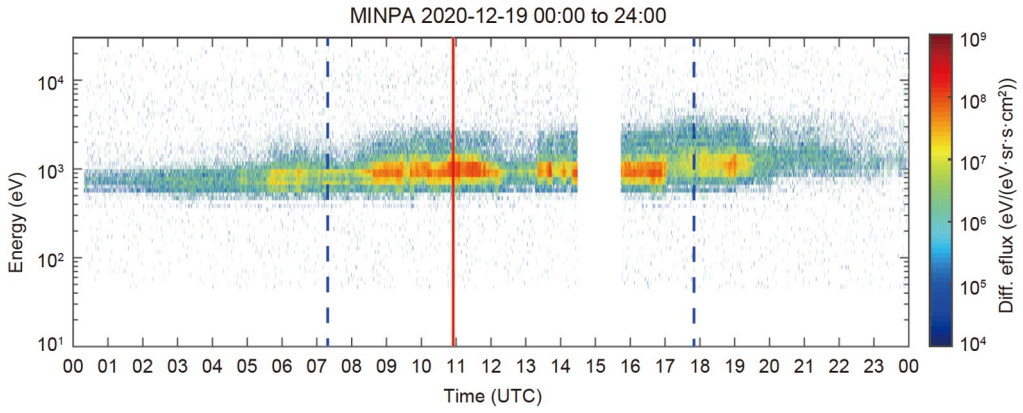

Figure 3 The energy spectrum of the solar wind observed on 12 December 2020. Colors denote the measured differential energy fluxes in eV/(eV·sr·s·cm^2) and the time given by the Coordinated Universal Time (UTC). The solid red line and blue dashed lines correspond to the fitting samples in Figure 4.

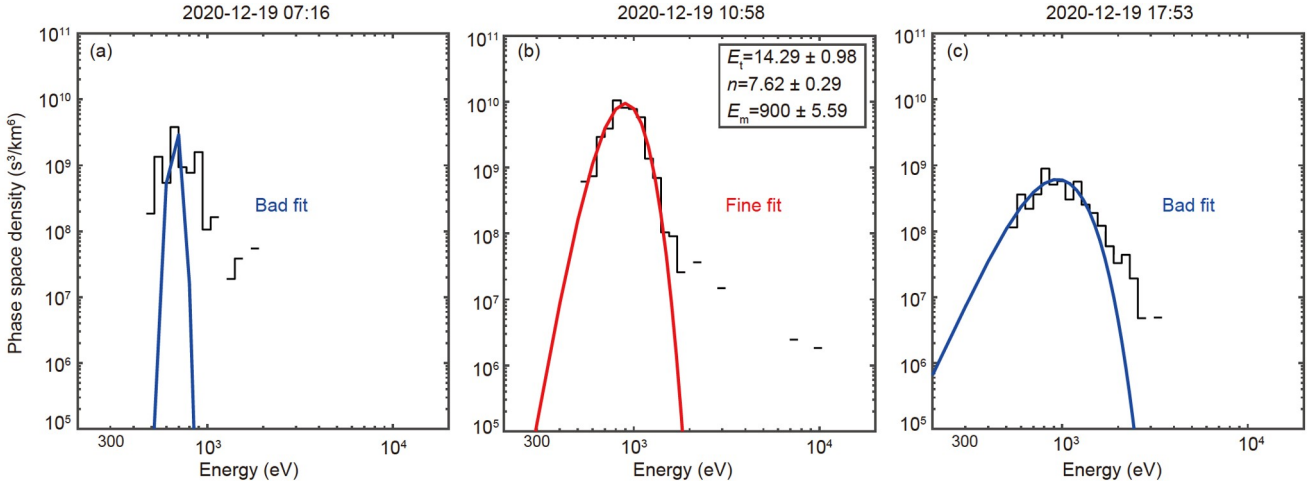

Figure 4 The PSD of H^+ was computed from MINPA datasets at 07:16, 10:58, and 17:53 UT. Data are sampled over 4 seconds. The black lines computed from the measured data. (a) & (c) The sheltered field of view results in bad fits shown as blue lines. (b) The red line denotes a good fit of a Gaussian distribution. Parameters resulting from the fit are thermal energy (E_t in eV), density (n in 1/cm^3), and mean energy (E_m in eV).

different locations: OMNI near-Earth and MAVEN at Mars while Tianwen-1 was approaching Mars. The solar wind parameters from OMNI and MAVEN were shifted and scaled to the position of Tianwen-1 spacecraft by assuming that the velocity is a constant and the density is decreasing by R^{-2}, where R is the heliocentric radial distance. The longitudinal and radial separations contribute to the time lag between Earth and Tianwen-1:

$$\Delta t = \frac{\phi_{ET}}{\omega} + \frac{R_T - R_E}{v_{SW}}, \tag{13}$$

where ϕ_{ET} is the angle between the Earth-Sun-Tianwen-1 lines, ω is the angular velocity of the solar rotation, R_T and R_E are the heliocentric radial distance of Earth and Tianwen-1, respectively; v_{sw} is the speed of the solar wind provided by OMNI datasets. The solar wind parameters at Mars observed by MAVEN were shifted to Tianwen-1 in the same way:

$$\Delta t = \frac{\phi_{MT}}{\omega} + \frac{R_T - R_M}{v_{SW}}, \tag{14}$$

where ϕ_{MT} is the Mars-Sun-Tianwen-1 angle, R_M is the heliocentric distance of Mars, v_{sw} is the solar wind velocity measured through MAVEN SWIA.

Tianwen-1 Observation from 31 October 2020 to 25 January 2021 shows that the interplanetary space environment between Mars and Earth is mainly composed of solar wind streams with different velocities and the SIRs with compressed plasma forming when fast streams overtake the preceding slower streams. The increase of the solar wind velocity during SIRs is successfully illustrated by MINPA.

Note that this time shift method is not applicable for relatively large longitudinal separations. Opitz et al. (2009, 2010) suggest that the time shift method considering the longitudinal and radial separations (eqs. (13) and (14)) is applicable when a longitudinal separation is less than 65° during the solar cycle 25. The included angle between Earth and Tianwen-1 ranged from 8° to 46° during the observation. We believe that the estimated time shift from Earth to Tianwen-1 is basically reliable. The estimated results are also accurate

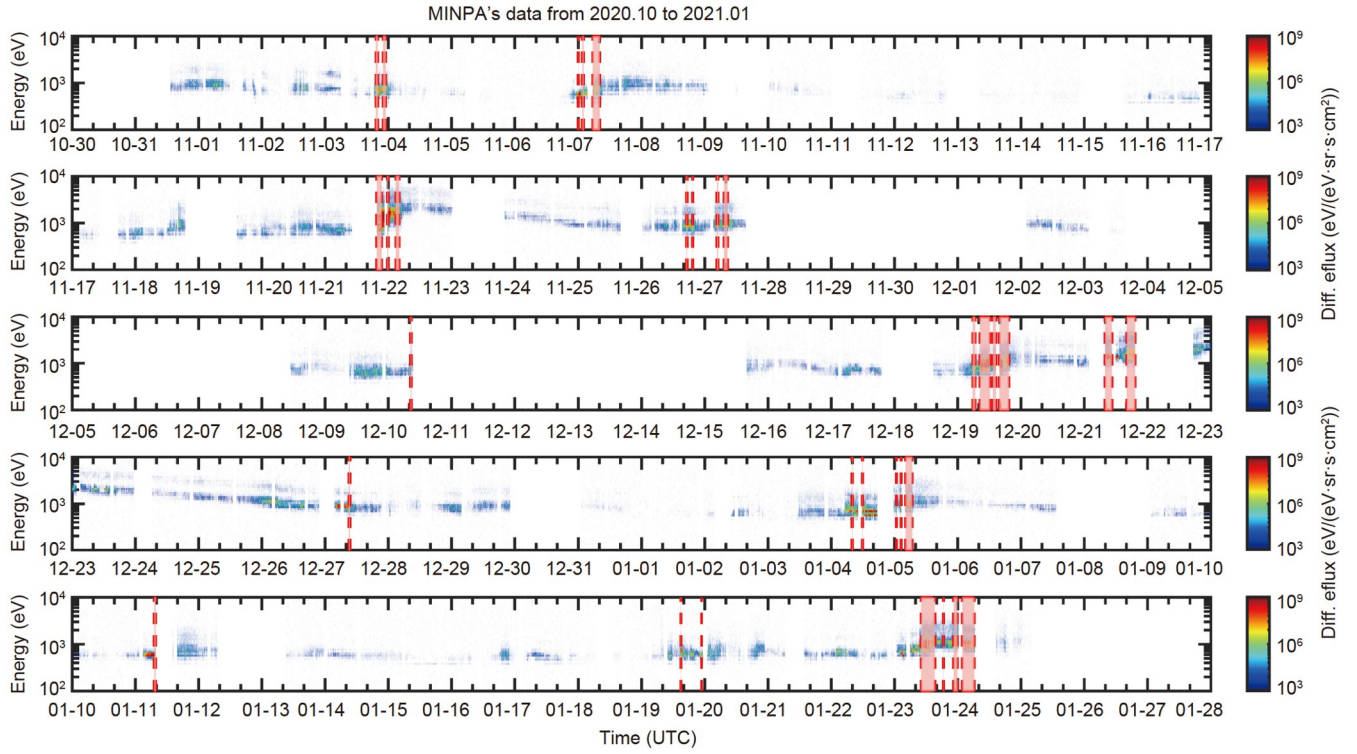

Figure 5 Energy spectra from MINPA in the cruise phase from 31 October 2020 to 25 January 2021. Colors denote the measured differential energy fluxes in eV/(eV·sr·s·cm^2) and the time given by UTC. The red dashed frames provide the reliable periods of datasets with the same fine-fitting as shown in Figure 4b.

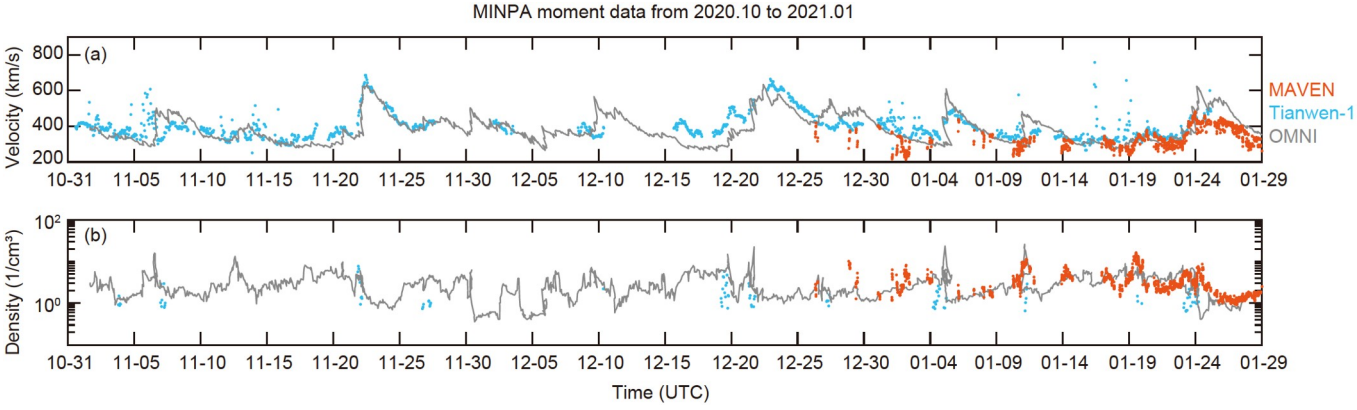

Figure 6 Velocity (a) and density (b) of the solar wind protons from Tianwen-1 (light blue), shifted MAVEN (orange), and shifted OMNI (grey) datasets from 31 October 2020 to 25 January 2021.

for the time shift from MAVEN to Tianwen-1 because they have an included angle of ~1°. However, due to the shielding effect, the solar wind densities from MINPA are highly underestimated (Zhang et al., 2022), limiting more detailed quantitative investigations of the solar wind properties.

4. Discussion

From 31 October 2020 to 25 January 2021, Tianwen-1 observed quiet solar wind with different speeds and SIRs with compressed plasma forming when fast streams overtake the preceding slower streams. During the cruise phase of the Tianwen-1 in the heliosphere, observations of SIRs appear several times, such as on 19 December 2020 and 5 January 2021 in Figure 5 and Figure 6, respectively. On 23 January 2021, Tianwen-1 is very close to Mars, as Figure 1 shows, providing a suitable chance to compare the solar wind observations between MINPA, SWIA, and STATIC. Figure 7 gives an example of the energy spectra based on each observation from 12:10 to 15:40 UT.

As shown by Figure 7a, the distance from Tianwen-1 to

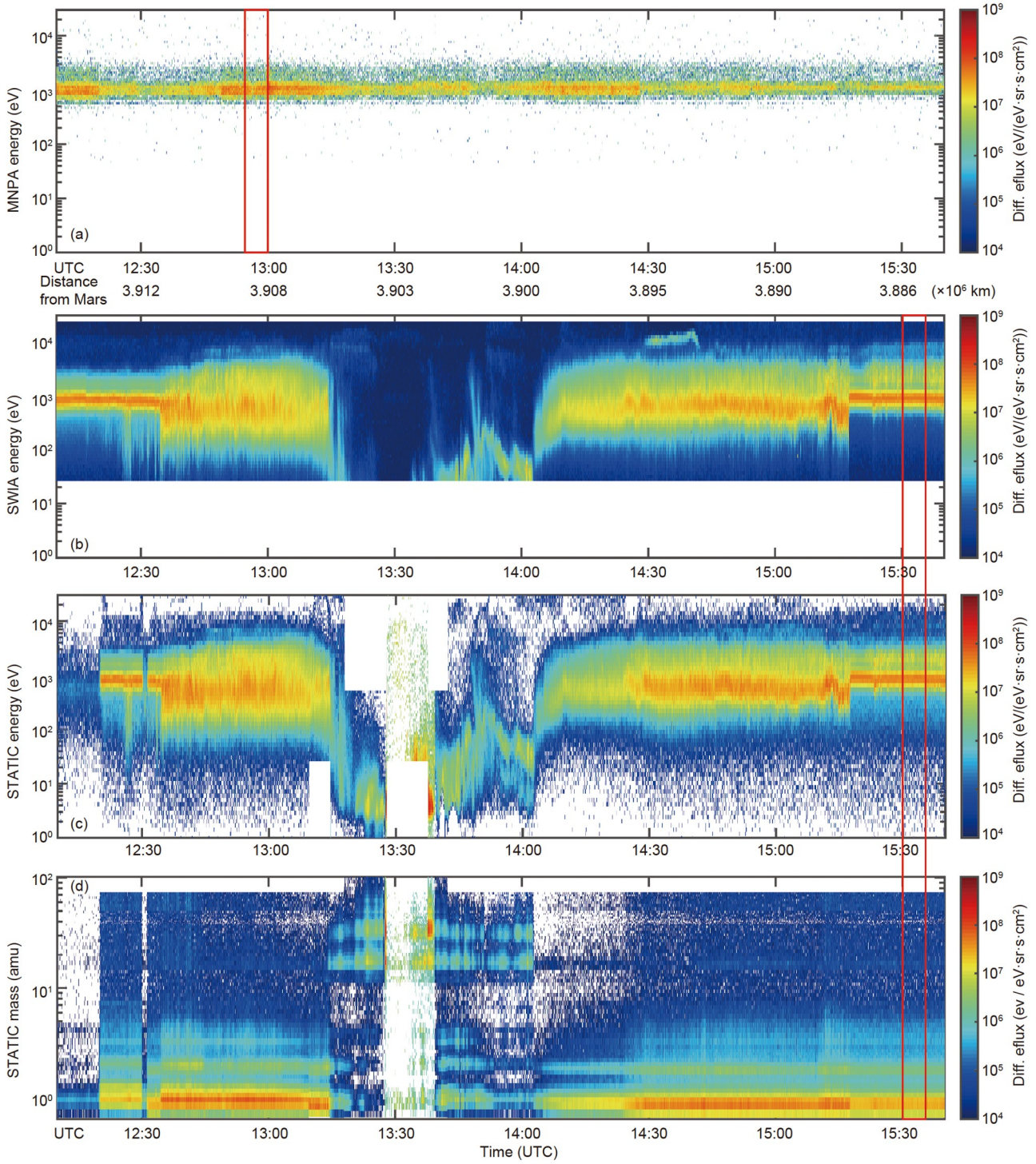

Figure 7 Ion energy spectrum from (a) MINPA, (b) SWIA, (c) STATIC, and (d) ion mass spectrum from STATIC from 12:10 to 15:40 on 23 January 2021 UT. The second line of the *x*-label in (a) provides the distance of Tianwen-1 from Mars in units of 10^6 km. Colors denote the measured differential energy fluxes in eV/(eV·sr·s·cm^2) and the time is given by UTC. Red boxes give periods during which the PSDs are calculated in Figure 8.

Mars during this time is near 3.9×10^6 km. The angles of Mars-Sun-Tianwen-1 are less than 1°. The Tianwen-1 and MAVEN are nearly radial alignment. The solar wind speed is 420 km/s in Figure 6a. It takes 155 minutes for the solar wind to propagate from Tianwen-1 to MAVEN. Thus, we choose periods both satellites could measure the solar wind, from 12:55 to 13:00 UT for Tianwen-1 and from 15:30 to 15:35 UT for MAVEN. The region is marked within the red boxes in Figure 7. The Helium ions in the solar wind observed through MAVEN STATIC in Figure 7d are not discussed here since no mass resolution data were available during the cruise phase. The PSDs are shown in Figure 8. The fitted

lines from the three different instruments are similar. The fitting factors of the three panels are within a similar tolerance scope; the density measured by MINPA is lower than the others, but its values are still comparable.

The results based on former Mars exploration missions such as Mars Express and MAVEN showed that the solar activities constrain ion escape rates (e.g., Nilsson et al., 2010; Brain et al., 2017). Plasma measurements near the Martian space could be obtained through Mars Express, MAVEN, and Tianwen-1 during their respective observation periods. We provide the records of the solar wind observations from Mars Express, MAVEN, and Tianwen-1 in Figure 9. Mars Express contributes eight-years observations on a total of 2462 orbits from the middle of the solar cycle 23 to the early half of the solar cycle 24 (Han et al., 2014). Observations of MAVEN start from October 2014, in a total of 8412 orbits, until October 2020, which also provide cross corrections for the Tianwen-1 measurements in Figure 6.

Statistically, the mean velocity of the solar wind from 2005 to 2020 is near 400 km/s, as well as its mean density is 1-2 protons/cm^3 from both Mars Express and MAVEN data in Figure 9a and 9b. Similar conclusions are reported by Ramstad et al. (2017) using 10 years of ASPRERA-3 IMA data from 2007 to 2017 and Liu et al. (2021) using 6 years of MAVEN SWIA measurements. These results suggest that the observations from Tianwen-1 within 26 million kilometers upstream of Mars from October 2020 to January 2021 in Figure 9c are consistent with the solar wind observations near Mars through Mars Express and MAVEN. As for further observations of heavy ions from the Martian lower atmosphere and energetic atoms, MINPA was restarted for its second continuous survey since 13 November 2021.

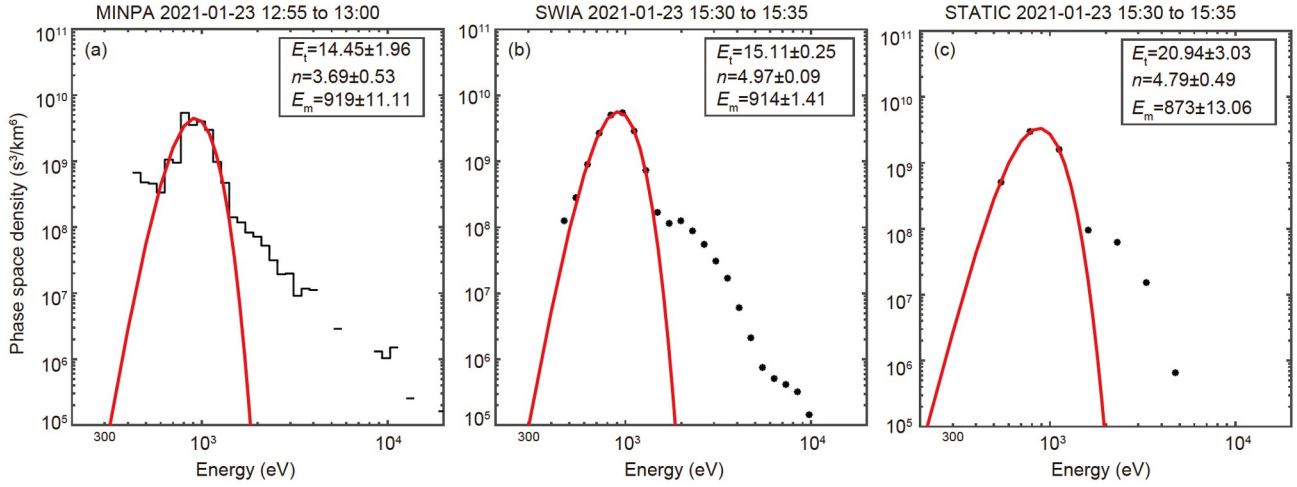

Figure 8 The PSD of H^+ computed from (a) MINPA datasets from 12:55 to 13:00 UT, 23 January 2021, and from (b) SWIA and (c) STATIC onboard MAVEN from 15:30 to 15:35 UT, 23 January 2021. Data are sampled over 5 minutes; the black lines (dots) are the measured data. The red line denotes a good fit for a Gaussian distribution. Fitted parameters are thermal energy (E_t in eV), density (n in 1/cm^3), and mean energy (E_m in eV).

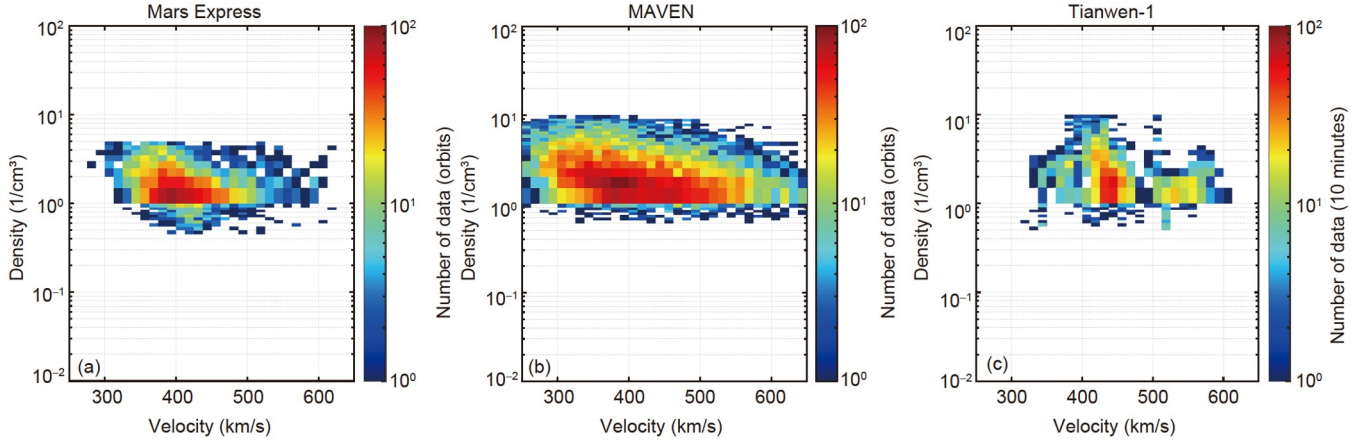

Figure 9 Comparison of proton densities and velocities between long-term solar wind observations near Mars made by (a) Mars Express (from April 2005 to July 2013, a total of 2462 orbits) and (b) MAVEN (from October 2014 to October 2020, a total of 8412 orbits) and (c) 3 months of MINPA *in-situ* data in the cruise phase during the transit to Mars (10 minutes averaged data).

5. Conclusions

From 31 October 2020 to 25 January 2021, MINPA finished its first 3-months measurements during the Tianwen-1's cruise phase, it provides a unique chance to jointly measure the solar wind from Earth to Mars. After reducing noises and filtering the sheltered datasets, we confirm the consistency of the solar wind plasma observations between Tianwen-1, OMNI, MAVEN, and Mars Express. In November 2021, MINPA restarted again for its secondary measurements within the Martian atmosphere after the cruise phase. We are looking forward to observing escaping ions and a possible multi-spacecraft campaign accompanied by Mars Express and MAVEN in the coming Martian years.

Acknowledgements *The Tianwen-1 data set is available at the Planet Exploration Program Scientific Data Release System (http://202.106.152.98:8081/marsdata/web/datainfo/). We acknowledge the use of NASA/GSFC's Space Physics Data Facility's OMNIWeb service and OMNI data. The MAVEN data are publicly available in NASA's Planetary Data System (https://pds-ppi.igpp.ucla.edu/mission/MAVEN). The authors would like to thank the MAVEN SWIA and STATIC teams for providing the data underlying this study. The authors thank the anonymous reviewers for their careful reading and insightful comments and suggestions. This work was supported by the Strategic Priority Research Program of the Chinese Academy of Sciences (Grant No. XDA17010201), the National Natural Science Foundation of China (Grant Nos. 42074207, 42104171), the Key Research Program of the Institute of Geology & Geophysics, CAS (Grant Nos. IGGCAS-201904, IGGCAS-202102), and the Key Research Program of Chinese Academy of Sciences (Grant No. ZDBS-SSW-TLC00103). Yong WEI is supported by the Thousand Young Talents Program of China. Limei YAN is supported by the Youth Innovation Promotion Association of CAS (Grant No. 2021064).*

References

Barabash S, Lundin R, Andersson H, Brinkfeldt K, Grigoriev A, Gunell H, Holmström M, Yamauchi M, Asamura K, Bochsler P, Wurz P, Cerulli-Irelli R, Mura A, Milillo A, Maggi M, Orsini S, Coates A J, Linder D R, Kataria D O, Curtis C C, Hsieh K C, Sandel B R, Frahm R A, Sharber J R, Winningham J D, Grande M, Kallio E, Koskinen H, Riihelä P, Schmidt W, Säles T, Kozyra J U, Krupp N, Woch J, Livi S, Luhmann J G, McKenna-Lawlor S, Roelof E C, Williams D J, Sauvaud J A, Fedorov A, Thocaven J J. 2006. The analyzer of space plasmas and energetic atoms (ASPERA-3) for the Mars express mission. Space Sci Rev, 126: 113–164

Barabash S, Fedorov A, Lundin R, Sauvaud J A. 2007. Martian atmospheric erosion rates. Science, 315: 501–503

Bavassano B, Pietropaolo E, Bruno R. 2001. Radial evolution of outward and inward Alfvénic fluctuations in the solar wind: A comparison between equatorial and polar observations by Ulysses. J Geophys Res, 106: 10659–10668

Brain D A, Barabash S, Bougher S W, Duru F, Jakosky B M, Modolo R. 2017. Solar wind interaction and atmospheric escape. In: Haberle R M, Clancy R T, Forget F, Smith M D, Zurek R W, eds. The Atmosphere and Climate of Mars. Cambridge: Cambridge University Press

Chi Y, Shen C, Luo B, Wang Y, Xu M. 2018. Geoeffectiveness of stream interaction regions from 1995 to 2016. Space Weather, 16: 1960–1971

Conlon T F. 1978. The interplanetary modulation and transport of Jovian electrons. J Geophys Res, 83: 541–552

Conlon T F, Simpson J A. 1977. Modulation of Jovian electron intensity in interplanetary space by corotating interaction regions. Astrophys J, 211: L45–L49

Dubinin E, Fränz M, Pätzold M, Woch J, McFadden J, Fan K, Wei Y, Tsareva O, Zelenyi L. 2020. Impact of martian crustal magnetic field on the ion escape. J Geophys Res Space Phys, 125: e2020JA028010

Dubinin E, Fränz M, Woch J, Roussos E, Barabash S, Lundin R, Winningham J D, Frahm R A, Acuña M. 2007. Plasma morphology at Mars. ASPERA-3 observations. Space Sci Rev, 126: 209–238

Fan K, Fränz M, Wei Y, Cui J, Rong Z, Chai L, Dubinin E. 2020. Deflection of global ion flow by the martian crustal magnetic fields. Astrophys J, 898: L54

Ferreira S E S, Potgieter M S, Burger R A, Heber B, Fichtner H. 2001. Modulation of Jovian and galactic electrons in the heliosphere: 1. Latitudinal transport of a few MeV electrons. J Geophys Res, 106: 24979–24987

Forbush S E. 1993. On World-Wide Changes in Cosmic-Ray Intensity. In: Van Allen J A, ed. Cosmic Rays, the Sun and Geomagnetism: The Works of Scott E. Forbush. 151–164

Fränz M, Dubinin E, Roussos E, Woch J, Winningham J D, Frahm R, Coates A J, Fedorov A, Barabash S, Lundin R. 2006. Plasma moments in the environment of Mars. Space Sci Rev, 126: 165–207

Fränz M, Harper D. 2002. Heliospheric coordinate systems. Planet Space Sci, 50: 217–233

Gazis P R. 1994. Pioneer and Voyager observations of solar cycle variations in the outer heliosphere. Geophys Res Lett, 21: 1743–1746

González-Esparza J A, Smith E J. 1996. Solar cycle dependence of the solar wind dynamics: Pioneer Voyager, and Ulysses from 1 to 5 AU. J Geophys Res, 101: 24359–24371

Halekas J S, Taylor E R, Dalton G, Johnson G, Curtis D W, McFadden J P, Mitchell D L, Lin R P, Jakosky B M. 2015. The solar wind ion analyzer for MAVEN. Space Sci Rev, 195: 125–151

Han X, Fränz M, Dubinin E, Wei Y, Andrews D J, Wan W, He M, Rong Z J, Chai L, Zhong J, Li K, Barabash S. 2014. Discrepancy between ionopause and photoelectron boundary determined from Mars Express measurements. Geophys Res Lett, 41: 8221–8227

Hutchinson I H. 2002. Principles of plasma diagnostics: Second edition. Plasma Phys Control Fusion, 44: 2603

Jakosky B M, Grebowsky J M, Luhmann J G, Connerney J, Eparvier F, Ergun R, Halekas J, Larson D, Mahaffy P, McFadden J, Mitchell D F, Schneider N, Zurek R, Bougher S, Brain D, Ma Y J, Mazelle C, Andersson L, Andrews D, Baird D, Baker D, Bell J M, Benna M, Chaffin M, Chamberlin P, Chaufray Y Y, Clarke J, Collinson G, Combi M, Crary F, Cravens T, Crismani M, Curry S, Curtis D, Deighan J, Delory G, Dewey R, DiBraccio G, Dong C, Dong Y, Dunn P, Elrod M, England S, Eriksson A, Espley J, Evans S, Fang X, Fillingim M, Fortier K, Fowler C M, Fox J, Gröller H, Guzewich S, Hara T, Harada Y, Holsclaw G, Jain S K, Jolitz R, Leblanc F, Lee C O, Lee Y, Lefevre F, Lillis R, Livi R, Lo D, Mayyasi M, McClintock W, McEnulty T, Modolo R, Montmessin F, Morooka M, Nagy A, Olsen K, Peterson W, Rahmati A, Ruhunusiri S, Russell C T, Sakai S, Sauvaud J A, Seki K, Steckiewicz M, Stevens M, Stewart A I F, Stiepen A, Stone S, Tenishev V, Thiemann E, Tolson R, Toublanc D, Vogt M, Weber T, Withers P, Woods T, Yelle R. 2015a. MAVEN observations of the response of Mars to an interplanetary coronal mass ejection. Science, 350: aad0210

Jakosky B M, Lin R P, Grebowsky J M, Luhmann J G, Mitchell D F, Beutelschies G, Priser T, Acuna M, Andersson L, Baird D, Baker D, Bartlett R, Benna M, Bougher S, Brain D, Carson D, Cauffman S, Chamberlin P, Chaufray J Y, Cheatom O, Clarke J, Connerney J, Cravens T, Curtis D, Delory G, Demcak S, DeWolfe A, Eparvier F, Ergun R, Eriksson A, Espley J, Fang X, Folta D, Fox J, Gomez-Rosa C, Habenicht S, Halekas J, Holsclaw G, Houghton M, Howard R, Jarosz M, Jedrich N, Johnson M, Kasprzak W, Kelley M, King T, Lankton M, Larson D, Leblanc F, Lefevre F, Lillis R, Mahaffy P, Mazelle C, McClintock W, McFadden J, Mitchell D L, Montmessin F, Morrissey J, Peterson W, Possel W, Sauvaud J A, Schneider N, Sidney W, Sparacino S, Stewart A I F, Tolson R, Toublanc D, Waters C, Woods T, Yelle R, Zurek R. 2015b. The Mars atmosphere and volatile evolution (MAVEN)

mission. Space Sci Rev, 195: 3–48
King J H, Papitashvili N E. 2005. Solar wind spatial scales in and comparisons of hourly Wind and ACE plasma and magnetic field data. J Geophys Res, 110: A02104
Kong L G, Zhang A B, Tian Z, Zheng X Z, Wang W J, Liu B, Wurz P, Piazza D, Etter A, Su B, An Y Y, Ding J J, Li W Y, Liu Y, Li L, Li Y R, Tan X, Sun Y Q. 2020. Mars Ion and Neutral Particle Analyzer (MINPA) for Chinese Mars Exploration Mission (Tianwen-1): Design and ground calibration. Earth Planet Phys, 4: 333–344
Lammer H, Kasting J F, Chassefière E, Johnson R E, Kulikov Y N, Tian F. 2008. Atmospheric escape and evolution of terrestrial planets and satellites. Space Sci Rev, 139: 399–436
Liu D, Rong Z, Gao J, He J, Klinger L, Dunlop M W, Yan L, Fan K, Wei Y. 2021. Statistical properties of solar wind upstream of Mars: MAVEN observations. Astrophys J, 911: 113
McFadden J P, Kortmann O, Curtis D, Dalton G, Johnson G, Abiad R, Sterling R, Hatch K, Berg P, Tiu C, Gordon D, Heavner S, Robinson M, Marckwordt M, Lin R, Jakosky B. 2015. MAVEN SupraThermal and Thermal Ion Compostion (STATIC) instrument. Space Sci Rev, 195: 199–256
Nilsson H, Carlsson E, Brain D A, Yamauchi M, Holmström M, Barabash S, Lundin R, Futaana Y. 2010. Ion escape from Mars as a function of solar wind conditions: A statistical study. Icarus, 206: 40–49
Nilsson H, Zhang Q, Stenberg Wieser G, Holmstrom M, Barabash S, Futaana Y, Fedorov A, Persson M, Wieser M. 2021. Solar cycle variation of ion escape from Mars. Icarus, https://doi.org/10.1016/j.icarus.2021.114610
Opitz A, Fedorov A, Wurz P, Szego K, Sauvaud J A, Karrer R, Galvin A B, Barabash S, Ipavich F. 2010. Solar-wind bulk velocity throughout the inner heliosphere from multi-spacecraft measurements. Sol Phys, 264: 377–382
Opitz A, Karrer R, Wurz P, Galvin A B, Bochsler P, Blush L M, Daoudi H, Ellis L, Farrugia C J, Giammanco C, Kistler L M, Klecker B, Kucharek H, Lee M A, Möbius E, Popecki M, Sigrist M, Simunac K, Singer K, Thompson B, Wimmer-Schweingruber R F. 2009. Temporal evolution of the solar wind bulk velocity at solar minimum by correlating the STEREO A and B plastic measurements. Sol Phys, 256: 365–377
Ramstad R, Barabash S, Futaana Y, Yamauchi M, Nilsson H, Holmström M. 2017. Mars under primordial solar wind conditions: Mars Express observations of the strongest CME detected at Mars under solar cycle #24 and its impact on atmospheric ion escape. Geophys Res Lett, 44: 10,805–10,811
Richardson I G. 2018. Solar wind stream interaction regions throughout the heliosphere. Living Rev Sol Phys, 15: 1
Simpson J A. 1998. Recurrent solar modulation of the galactic cosmic rays and the anomalous nuclear component in three dimensions of the heliosphere. Space Sci Rev, 83: 7–19
Söding A, Neubauer F M, Tsurutani B T, Ness N F, Lepping R P. 2001. Radial and latitudinal dependencies of discontinuities in the solar wind between 0.3 and 19 AU and −80° and +10°. Ann Geophys, 19: 667–680
Wan W X, Wang C, Li C L, Wei Y. 2020a. China's first mission to Mars. Nat Astron, 4: 721
Wan W X, Wang C, Li C L, Wei Y, Liu J J. 2020b. The payloads of planetary physics research onboard China's First Mars Mission (Tianwen-1). Earth Planet Phys, 4: 331–332
Wei Y, Fränz M, Dubinin E, Woch J, Lühr H, Wan W, Zong Q G, Zhang T L, Pu Z Y, Fu S Y, Barabash S, Lundin R, Dandouras I. 2012. Enhanced atmospheric oxygen outflow on Earth and Mars driven by a corotating interaction region. J Geophys Res, 117: A03208
Wüest M, Evans D S, von Steiger R. 2007. Calibration of Particle Instruments in Space Physics. SR-007, Published for The International Space Science Institute by ESA Communications, Noordwijk, T
Zhang A B, Kong L G, Li W Y, Li L, Tang B B, Rong Z J, Wei Y, Ma J J, Zhang Y T, Xie L H, Wang Y X, He J S, Liu B, Wang W J, Su B, Li J W, Tan X, Wang F, Jin T F, Qiao F H, Wurz P, Zhu Y, Bai Y F, Li Y R, Zhu X B, Sun Y Q, Zou Y L, Wang C. 2022. Tianwen-1 MINPA observations in the solar wind. Earth Planet Phys, 6: 1–9
Zhang J, Liemohn M W, Kozyra J U, Thomsen M F, Elliott H A, Weygand J M. 2006. A statistical comparison of solar wind sources of moderate and intense geomagnetic storms at solar minimum and maximum. J Geophys Res, 111: A01104
Zou Y, Zhu Y, Bai Y, Wang L, Jia Y, Shen W, Fan Y, Liu Y, Wang C, Zhang A, Yu G, Dong J, Shu R, He Z, Zhang T, Du A, Fan M, Yang J, Zhou B, Wang Y, Peng Y. 2021. Scientific objectives and payloads of Tianwen-1, China's first Mars exploration mission. Adv Space Res, 67: 812–823

(Responsible editor: Xueshang FENG)